Chemical Science

ROYAL SOCIETY OF CHEMISTRY

EDGE ARTICLE

View Article Online
View Journal | View Issue

Cite this: *Chem. Sci.*, 2023, **14**, 4817

All publication charges for this article have been paid for by the Royal Society of Chemistry

Multiple responses of 1,6-diphenyl-1,3,5-hexatriene to mechanical stimulation: emission enhancement, piezochromism and negative linear compressibility†

Zhiyuan Fu,[a] Zhiqiang Yang,[b] Xinyi Yang,[a] Kai Wang *[ac] and Bo Zou *[a]

Received 29th January 2023
Accepted 29th March 2023

DOI: 10.1039/d3sc00482a

rsc.li/chemical-science

The properties of mechanoresponsive materials are mainly affected by intermolecular interaction, in which anisotropic grinding and hydrostatic high-pressure compression are the powerful tools used for modulation. Upon applying high pressure to 1,6-diphenyl-1,3,5-hexatriene (DPH), the reduced molecular symmetry results in the originally forbidden $S_0 \rightarrow S_1$ transition to become allowed that then leads to a 13-times emission enhancement, and π–π interactions result in piezochromism (red-shifted up to 100 nm). With increasing pressure, high-pressure-stiffened H···C/C···H and H···H interactions enable the DPH molecules to generate a NLC mechanical response (9–15 GPa) with $K_b = -5.8764\ \mathrm{TPa}^{-1}$ along the *b*-axis. As a contrast, upon destroying the intermolecular interactions by grinding, the DPH luminescence blue-shifts from cyan to blue. Based on this research, we investigate a new pressure-induced emission enhancement (PIEE) mechanism and enabled NLC phenomena by controlling weak intermolecular interactions. In-depth research of the evolution of intermolecular interactions has important reference value for developing new fluorescence materials and structural materials.

Introduction

Mechanoresponsive materials, mainly affected by intermolecular interaction, have attracted researchers' attention due to their great potential application value in various fields,[1–4] especially the optical and structural properties of materials. The impact of intermolecular interactions on optical properties is significant. For example, organic mechanochromic luminescence (MCL) materials have been widely studied for their important applications in data storage, sensors, encryption, anti-forgery, fluorescence probes *etc.*[5–11] In related studies, organic luminescent materials exhibit highly similar phenomena upon anisotropic grinding and hydrostatic high-pressure compression. For example, research on benzothiazole-enamido boron difluoride complexes,[12] Tetraphenylethylene derivatives,[13] Py-BP-PTZ,[14] boron diketonate[15] and BP2VA[16] found that the compounds exhibited an emission red-shift due to π–π interaction, the planarization of molecular conformation or the intramolecular charge transfer (ICT) effect depending on whether the samples were subjected to high pressure or grinding. Differently, 2,3,4,5-tetra(2-thiazolyl) thiophene showed a fluorescence blue-shift after grinding and a red-shift under high pressure. The suppression of excimer formation by grinding and the formation of dimers under high pressure were the main reasons for this phenomenon. The co-crystal CT-R exhibited the same phenomenon, wherein grinding led to a rearrangement of the co-crystal structure, resulting in weakening of the π–π and charge transfer interactions, whereas high pressure enhances these interactions.[17,18] In these MCL materials, intermolecular interactions will not only cause a change of the luminescence color, but also the emission intensity. For pressure-induced emission enhancement (PIEE), researchers have mostly focused on the propeller-shaped or shell-shaped molecules, such as tetraphenylethylene (TPE),[19] 1,2,3,4-tetraphenyl-1,3-cyclopentadiene (TPC),[20] triphenylamine (TPA),[21] carbazole,[22] *etc.*, and the mechanism was explained by the restriction of intramolecular motion (RIM), in which high pressure can restrict the motion of the molecule by regulating intermolecular interactions, leading to attenuation of the non-radiative transition rate. From an in-depth study on PIEE, Yang *et al.*[23] found that the rehybridization of N atoms could trigger a molecular conformational transition to induce the PIEE phenomenon. Tian *et al.*[24] reported that changing the molecular conformation using high pressure resulted in a switching of

[a]*State Key Laboratory of Superhard Materials, College of Physics, Jilin University, Changchun 130012, P. R. China. E-mail: kaiwang@jlu.edu.cn; zoubo@jlu.edu.cn*

[b]*State Key Laboratory of Supramolecular Structure and Materials, College of Chemistry, Jilin University, Changchun 130012, P. R. China*

[c]*Shandong Key Laboratory of Optical Communication Science and Technology, School of Physics Science and Information Technology, Liaocheng University, Liaocheng 252000, P. R. China*

† Electronic supplementary information (ESI) available: Experimental details, crystal structure, aggregation experiment, UV-vis absorption and grinding experiment. See DOI: https://doi.org/10.1039/d3sc00482a

excited state characteristics of the molecule to induce a fluorescence enhancement. Since there is a relationship between the PIEE phenomenon and the excited state energy, PIEE can also be achieved by changing a forbidden transition into an allowed transition. This will greatly expand the mechanism scope of PIEE.

The influence of intermolecular interactions on the structure is not as significant as that on the optical properties. We need to observe it from the microscopic crystal lattice. Under hydrostatic high pressure, some crystal lattices produce a negative compressibility along the crystal axis whereby the volume is continuously compressed under high pressure, which is called negative linear compressibility (NLC).[25] So far, only a few NLC materials have been discovered and the NLC behavior is concentrated in the low pressure region (<5 GPa), such as $[NH_4][Zn(HCOO)_3]$,[26] $Zn[Au(CN)_2]_2$,[27] $Ag_3[Co(CN)_6]$,[28] and ammonium oxalate monohydrate.[29] These NLC materials are mainly based on framework-structured molecules, and the mechanical response of hydrogen bonds or chemical bonds is the main reason for NLC.[30–32] In organic crystals, besides the hydrogen bonds and chemical bonds, there are many different intermolecular interactions. Utilizing these numerous intermolecular interactions to generate NLC phenomena will greatly broaden the research scope of NLC materials.[25] Given all that, the intermolecular interactions occurring under different pressures will have different effects on various properties of the material. In-depth research on the evolution of intermolecular interactions has important reference value for developing new fluorescence materials and structural materials. Considering the issue mentioned above, pressure is a powerful means of regulation of intermolecular interactions. Herein, to clearly study the emission change and structure evolution of organic molecules with increasing pressure, a linear molecule, 1,6-diphenyl-1,3,5-hexatriene (DPH), was chosen as an ideal research object, due to its simple molecule structure and plain intermolecular interactions.

Results and discussion

The DPH crystal crystallizes in the orthorhombic *Pbca* space group; molecules are stacked parallel along the *b*-axis and cross-aligned head-to-head along the *c*-axis in each layer, showing a W-shape. The layer extends along the *a*-axis (Fig. S1†). DPH is a unique fluorescent material; due to its centrosymmetrical nature and C_{2h} point group, S_0 and S_1 of DPH are both ^1Ag, resulting in the fact that S_1 is symmetry forbidden according to the Laporte rule.[33–35] S_1 obtains oscillator strength through Herzberg–Teller coupling, and from there most of the emission occurs.[35] Fig. 1a and b show the emission spectra and fluorescence photos of DPH crystals at different pressures. At ambient pressure, the DPH crystal exhibited a weak cyan emission. When applying hydrostatic high pressure to the DPH crystal using a diamond anvil cell (DAC), the emission intensity at 4 GPa was 13 times that of the original and the fluorescence color red-shifted from weak cyan to bright green. Based on the excitation spectra of DPH (Fig. S2†), we ruled out the effect of the excitation spectra changing with pressure on the emission

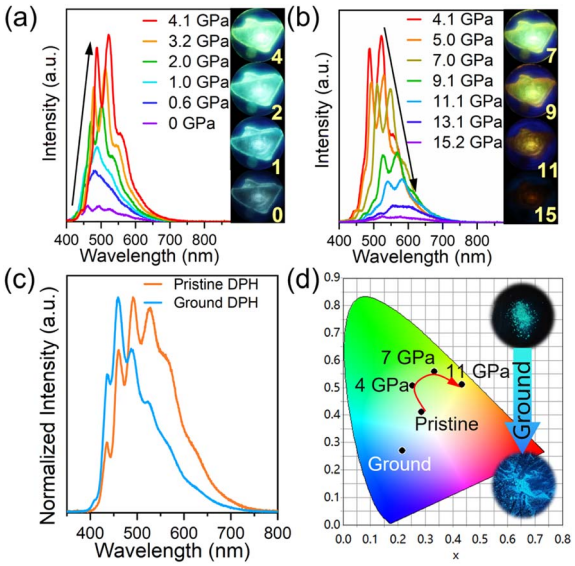

Fig. 1 (a, b) Emission spectra and photos of the DPH crystal at different pressures. The yellow numbers on the photos represent the pressure (unit: GPa). (c) Emission spectra of DPH before and after grinding. (d) Corresponding International Commission on Illumination chromaticity diagram of DPH before and after grinding. The inset shows the corresponding photos.

intensity. With increasing pressure, the emission intensity decreased while the fluorescence color red-shifted to weak brownish-yellow continually. Since the DPH molecule has a rigid planar structure without the influence of heteroatoms, the emission enhancement phenomenon is abnormal for DPH. More interestingly, when we put crystalline DPH powder into an agate mortar for grinding, the fluorescence color of the DPH powder blue-shifted from cyan to blue, as shown in Fig. 1c and d. It showed a completely different phenomenon from that under high pressure. We performed verification experiments in which DPH molecules were induced to aggregate, and the results showed that DPH did not exhibit aggregation-induced emission (AIE) (Fig. S4†). Furthermore, the fluorescence quantum yield (QY) of DPH crystals was only 2.27%, while that of DPH in pure THF solution was as high as 41.56%. These results meant that the emission enhancement of DPH could no longer be explained by the traditional RIM mechanism.

To clearly analyze the reasons for such emission responses and observe the evolution of intermolecular interactions between DPH molecules, we performed Raman, infrared (IR) and angle dispersive X-ray diffraction (ADXRD) measurements on the DPH crystal. Fig. 2a and b and S5† show the high-pressure Raman spectra of the DPH crystal, and the Raman peaks in the range of 50–400 cm^{-1} were all assigned to the bending vibration of C–C=C in DPH.[36] With increasing pressure, the Raman peaks almost all moved towards higher wavenumbers, but these peaks had different shift rates. The peak at 194.29 cm^{-1} shifted to 192.64 cm^{-1} first at 0.5 GPa and then shifted to higher wavenumbers. And the peaks at 105 cm^{-1} and 188 cm^{-1} split at 1 GPa and 2.5 GPa, respectively. This indicated that the C–C=C skeleton of DPH underwent a deformation

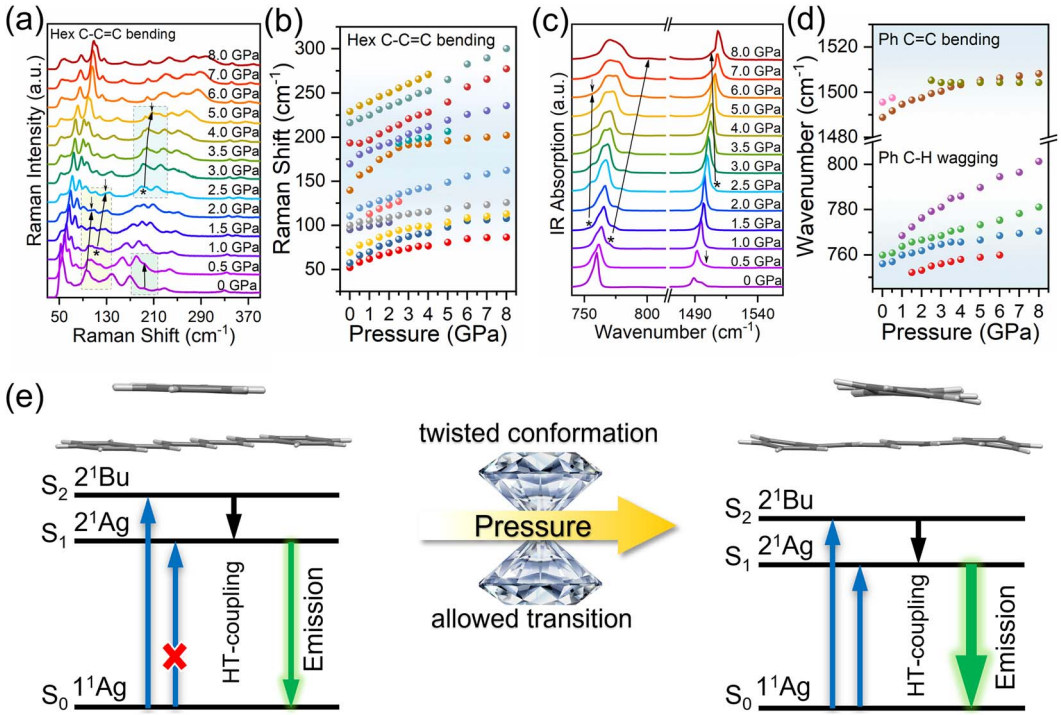

Fig. 2 (a) The Raman spectra of DPH at different pressures and (b) the pressure dependence of Raman peaks of the C–C=C vibrational modes. (c) The IR spectra of DPH, and (d) the corresponding wavenumber of C–H and C=C peaks at different pressures. Ph represents phenyl ring, and Hex represents hexatriene, which are both part of DPH. "*" represents the appearance of new peaks, and "↓" means the disappearance of peaks. (e) Schematic diagram of molecular conformational distortion and allowed transition under high pressure.

during the compression.[37,38] In the IR spectra, the peaks at 695 cm^{-1}, 756 cm^{-1} and 760 cm^{-1} were assigned to the C–H wagging of the phenyl ring part of DPH, the peaks located at 995 cm^{-1} and 1005 cm^{-1} belong to the C–H wagging of hexatriene, and the peaks at 1489 cm^{-1} and 1496 cm^{-1} represent the C=C bending of phenyl rings, as shown in Fig. 2c, d and S6.†[36] Obviously, these IR absorption peaks split and broadened, accompanied with different shift rates, which indicated that the hexatriene of DPH underwent molecular deformation and the benzene ring also became distorted during the compression. To further verify the occurrence of molecular deformation, we studied the changes of the lattice parameters based on *in situ* high-pressure ADXRD. According to the ADXRD patterns, the diffraction peaks (Fig. S7a†) moved to higher angles and no new peaks appeared, which indicated that the DPH crystal did not undergo a phase transition during the compression process. In the range of 0–8 GPa, the *a*-axis had the highest compression ratio, while the *b*-axis had the smallest compression ratio (Fig. S7b†). Different compression ratios caused the DPH molecules to experience different interaction strengths along different lattice axes, resulting in deformation of the DPH molecule. We also performed first-principles calculations and obtained the structure of the DPH crystal under high pressure. The results showed that the symmetry of the DPH molecule changed from C_{2h} under ambient conditions to C_i at high pressure. In other words, the molecular symmetry of DPH at high pressure decreased. Although the calculated molecular structure still remains centrosymmetric, in fact, the inherently asymmetric vibrations caused the DPH molecules to continuously deform and become non-centrosymmetric molecules in an instantaneous state. With increasing pressure, the probability that asymmetric vibrations caused DPH to become a non-centrosymmetric molecule was enhanced. According to the Laporte rule, the forbidden transition will be weakly allowed due to the existence of asymmetric vibrations in centrosymmetric molecules.[39] As a result, with the increasing pressure, the probability of the $S_0 \rightarrow S_1$ transition caused by the asymmetric vibration gradually increased. Compared with the oscillator strength obtained only by coupling, the allowed transition of $S_0 \rightarrow S_1$ caused S_1 to gain more energy to emit enhanced fluorescence under high pressure (Fig. 2e). At higher pressure (after 4 GPa), as the intermolecular distances were compressed, the interactions between adjacent molecules, especially the π–π interactions (Fig. S8†), were gradually enhanced, which reduced the energy of the lowest excited state (Fig. S9†) and the radiative transition rate, resulting in a red-shift in the wavelength and a decrease in emission intensity.[40–43]

Unlike the evolution under high pressure, neither the IR spectra nor Raman spectra (Fig. S10a and b†) of the ground DPH powder showed significant differences compared to the initial DPH powder. The XRD diffraction peaks of the ground DPH powder were broadened, and some peaks merged (Fig. S10c†), which meant that the crystallinity of the powder sample was reduced. Also, the emission spectra of the ground DPH powder (Fig. S10d†) were located between the emission spectra of the monodisperse solution (see the aggregated

experiment, 5×10^{-5} mol L^{-1}) and that of the crystal. Relative to the DPH crystal, the blue-shifted luminescence of the ground DPH powder was caused by the decreased crystallinity of the DPH powder sample because the loose packing mode and intra-layer W-shape arrangement of the DPH crystal made the weak intermolecular interactions more easily disrupted by anisotropic grinding. This result made the stacking mode more inclined to lose order after grinding, producing a luminescence similar to that of the monodisperse solution. To avoid the impact caused by the possible *J*-aggregate state or *H*-aggregate state transformation, we compared the UV-Vis absorption spectra after grinding with that of the crystal, and the results showed that there was no aggregation state transformation during the grinding process (Fig. S10e†). Furthermore, we also performed grinding fluorescence experiments on *trans*-Stilbene (TSB) and *trans*,*trans*-1,4-diphenyl-1,3-butadiene (DPB) (Fig. S10f†). Due to their shorter ethylene chains, the packing mode is more compact than that of DPH, so their fluorescence spectra after grinding showed almost no changes. In a word, regarding the hydrostatic pressure and anisotropic force on the DPH crystal, the evolution of intermolecular interactions and the packing mode of the DPH crystal resulted in distinct mechanochromic luminescence responses.

Regarding the DPH crystal structure, the lattice axis of the DPH crystal exhibited different rates of compression in the range of 0–9 GPa. Unusually, when pressure exceeded 9 GPa and up to the highest pressure of 15 GPa that we could measure (Fig. S7a†), the diffraction peak of the (020) plane shifted towards a lower 2-theta angle in the ADXRD patterns. To gain insight into this anomalous phenomenon, forcefield, DFT and Hirshfeld surface calculations were performed under high pressure. We used the COMPASS forcefield to calculate the non-bond energy of the DPH crystal (Fig. S11†). The results show that the non-bond energy in the first 6 GPa has negative values (lower than 0 kcal mol^{-1}), indicating that the molecules are in a state of mutual attraction, which corresponds to the distortion of molecular conformation caused by the intermolecular interaction during the emission enhancement. Subsequently, the non-bond energy values become positive and increase rapidly after 6 GPa. The molecules shift from the mutual attraction state to a mutual repulsion state. Fig. 3 show the Hirshfeld surface and fingerprint plot. On the Hirshfeld surface, the larger and the darker the red area, the stronger the interaction. d_e and d_i on the fingerprint plot represent the distance from a point on the Hirshfeld surface to the nearest nucleus outside and inside the surface, respectively.[44] At ambient pressure, the Hirshfeld surface mainly consists of C···H/H···C and H···H, and there were only a few tiny red areas due to the large intermolecular distances, which were ascribed to C···H/H···C interactions. When pressure was increased up to 9 GPa, the fingerprint plot of DPH moved significantly to the lower left corner, and large and dark red areas appeared on the Hirshfeld surface, which meant abundant C···H/H···C and H···H interactions between the molecules and that they strengthened with the increasing pressure. Although the C···C interactions appeared, they were weak due to their location in the upper right corner of the fingerprint. Mainly C···H/H···C and H···H interactions dominate the structural properties of DPH.

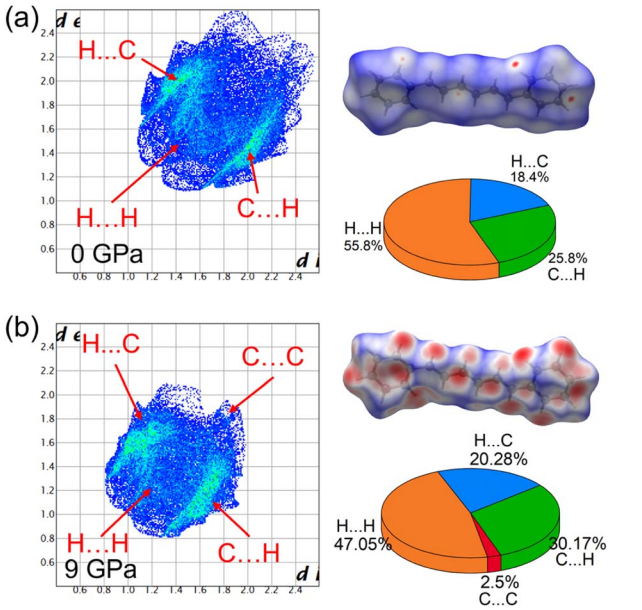

Fig. 3 Hirshfeld surface and fingerprint plot for the calculated structure at (a) 0 and (b) 9.0 GPa mapped with d_{norm}. The pie charts show the proportion of intermolecular interactions.

Fig. 4a shows the compression rate of the lattice axis changing with pressure. In the range of 9–15 GPa, the *b*-axis was continuously elongated by 2.84%. The compressibility of the lattice parameters in the range of 9–15 GPa was calculated by the PAScal program,[45] and the results were $K_a = 11.7879$ TPa^{-1}, $K_b = -5.8764$ TPa^{-1} and $K_c = 5.3036$ TPa^{-1}, respectively. This clearly showed the NLC of the DPH crystal along the *b*-axis. The calculated results are shown in Fig. 4b. The *b*-axis elongated with increasing pressure after 9 GPa, which was in agreement with the experimental results. Considering that the DPH crystal shows a layered packing structure extending along the *a*-axis, there was enough space between the layers for compression, which led to the maximum compressibility along the *a*-axis (Fig. S7b†). Moreover, in the initial state, the intermolecular distances in the layers along the *c*-axis were too long to form stiffened interactions, and there was sufficient space for the molecules to move closer to each other. Therefore, during the compression of 0–9 GPa, the *a*-, *b*- and *c*-axes were all compressed. As the pressure continuously increased, the compressibility of the *c*-axis began to decrease after 10 GPa (Fig. S7b†), indicating that the DPH molecules along the *c*-axis were unable to get closer to each other due to the stiffened C–H···C and H···H interactions. The phenomenon that the vibration spectra of the C–H bending vibration shifted to lower wavenumbers (Fig. S12†) confirmed the "stiffening" process of C–H···C and H···H interactions. At the same time, due to the W-shape arrangement, the DPH molecules could slip along the *b*-axis due to the mechanical response of these interactions. The distance of d_{C-H} (Fig. 4c) decreased with increasing pressure before 9 GPa, and then increased after 9 GPa, which was

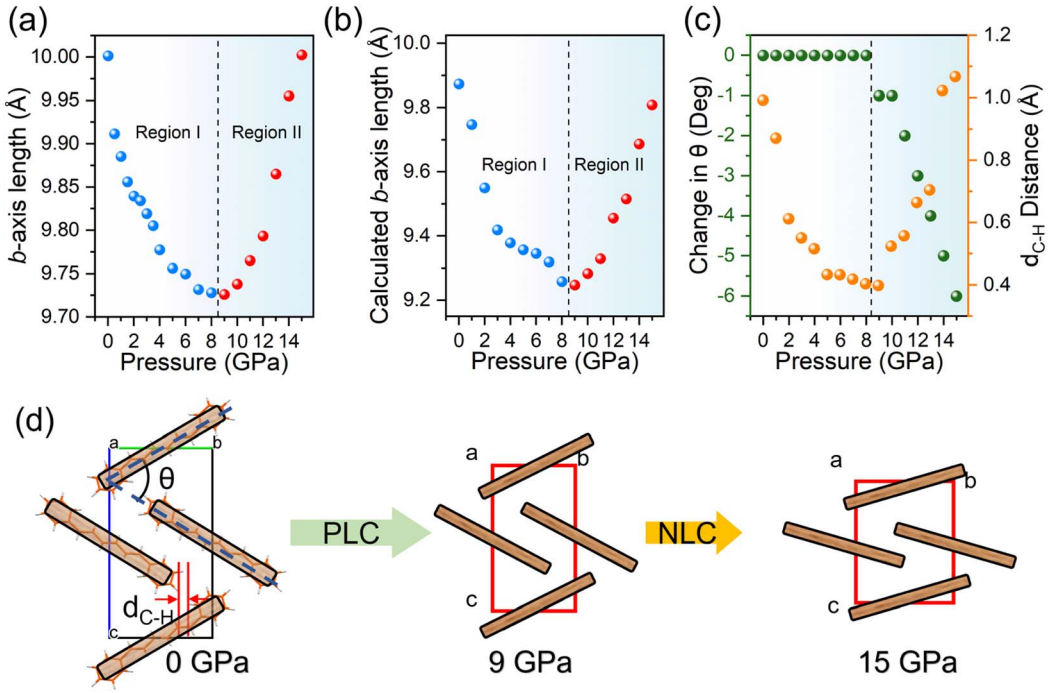

Fig. 4 (a) Pressure-dependent *b*-axis length of the DPH crystal up to 15 GPa. (b) Pressure-dependent calculated *b*-axis length of the DPH crystal up to 15 GPa. (c) The calculated intermolecular angle θ and distances at different pressures. (d) Schematic of PLC and NLC processes at 0, 9 and 15 GPa, respectively.

consistent with the occurrence of NLC along the *b*-axis. In addition, the decreased θ after 9 GPa (Fig. 4c) was similar to that of the wine-rack motif NLC material. These two factors together led to the NLC of the DPH crystal, as shown in the schematic diagram in Fig. 4d.

According to the analysis above, the intermolecular interaction has a pre-compression strengthening process. Thus, the organic NLC materials are first compressed (positive linear compressibility, PLC) and then NLC occurred. Before the critical pressure of the NLC phenomenon, the strength of intermolecular interactions is much weaker than the "hard" chemical bonds and hydrogen bonds in NLC materials such as MOFs. As the pressure increases, the strength of these interactions will gradually increase until they are strong enough to produce a mechanical response. For example, in an early report on methanol monohydrate, low temperature played a role of preload strengthening on the hydrogen bonds at ambient pressure, and the *a*-axis elongated with the increase of pressure at 160 K.[46] Besides, a similar phenomenon appeared in ammonium oxalate monohydrate that needed 4 GPa to preload strengthen the hydrogen bonds.[29] In general, the special intra-layer W-shape packing mode and the "long-chain" conformation of DPH molecules were the main fountainhead of NLC. We can also conclude that even weak interactions such as C–H···C and H···H can become "stiffening" under high pressure to produce a mechanical response. On these grounds, this kind of NLC mechanism can be extended to more organic materials.

Conclusions

In conclusion, taking DPH as an example, we investigated the effect of intermolecular interactions on material properties under anisotropic grinding and different hydrostatic high pressures. Under anisotropic grinding, the weak intermolecular interactions were easily disrupted, leading to a decrease in crystallinity, which made the DPH fluorescence blue-shift, similar to that of the monodisperse solution. When the hydrostatic pressure was relatively low, DPH contained different intermolecular interactions along different lattice axes, resulting in the molecular symmetry of DPH decreasing, which made the probability of the $S_0 \rightarrow S_1$ transition caused by asymmetric vibration gradually increase. As a result, DPH exhibited a 13-times emission enhancement at hydrostatic pressures of 0–4 GPa. A red-shift and reduced emission intensity were mainly caused by π–π interactions. With increased pressure, high-pressure-stiffened H···C/C···H and H···H interactions, guided by the intra-layer W-shape packing mode, enable DPH molecules to generate NLC mechanical responses along the *b*-axis. This enabled DPH to achieve an NLC mechanical response of $K_b = -5.8764\ \mathrm{TPa}^{-1}$ in the range of 9–15 GPa. The in-depth research on intermolecular interactions not only proposes a new PIEE mechanism but proves that weak intermolecular interactions can also generate NLC. These findings provide important reference value for the development of new materials such as fluorescent materials and structural materials.

Data availability

The datasets supporting this article have been uploaded as part of the ESI.†

Author contributions

Zhiyuan Fu: the conceptualization, methodology, validation, formal analysis, investigation and writing (original draft). Zhiqiang Yang: investigation. Xinyi Yang: supervision. Kai Wang: supervision, writing (review & editing). Bo Zou: supervision, project administration.

Conflicts of interest

There are no conflicts to declare.

Acknowledgements

This work is supported by the National Natural Science Foundation of China (NSFC) (No. 12174146 and 21725304), the fundamental research funds for the Central Universities, and the Special Construction Project Fund for Shandong Province Taishan Scholars. ADXRD experiments were performed at the 4W2 beamline at Beijing Synchrotron Radiation Facility (BSRF).

References

1 P. Yang, F. Zhu, Z. Zhang, Y. Cheng, Z. Wang and Y. Li, Stimuli-responsive polydopamine-based smart materials, *Chem. Soc. Rev.*, 2021, **50**, 8319–8343.

2 R. Xiong, R. X. Xu, C. Huang, S. De Smedt and K. Braeckmans, Stimuli-responsive nanobubbles for biomedical applications, *Chem. Soc. Rev.*, 2021, **50**, 5746–5776.

3 J. Zhang, B. He, Y. Hu, P. Alam, H. Zhang, J. W. Y. Lam and B. Z. Tang, Stimuli-Responsive AIEgens, *Adv. Mater.*, 2021, **33**, 2008071.

4 X. Wen, R. Sha and J. Wang, Research Progress of Stimuli-responsive AIE-active Hydrogels, *Chin. J. Lumin.*, 2022, **43**, 642–661.

5 H. Sun, W. H. Sun, Y. Jiang, J.-H. Wei, Y. Zhao, R. Zhang and Z.-H. Ni, Multi-stimuli-responsive tetraphenylethene-based thiazole compound: Time-dependently enhanced blue-shift emission, reversible acidichromism and mechanochromism, *Dyes Pigm.*, 2020, **173**, 107938.

6 H. Zhou, X. Feng, Z. Guo, Z. Zhuang, S. Fu, X. Liu and D. Xu, Design, synthesis, and mechanochromic luminescence of twisted donor–acceptor bisarylic methanone derivatives, *J. Lumin.*, 2022, **248**, 118966.

7 H. Traeger, D. J. Kiebala, C. Weder and S. Schrettl, From Molecules to Polymers—Harnessing Inter- and Intramolecular Interactions to Create Mechanochromic Materials, *Macromol. Rapid Commun.*, 2021, **42**, 2000573.

8 C. H. Barty-King, C. L. C. Chan, R. M. Parker, M. M. Bay, R. Vadrucci, M. De Volder and S. Vignolini, Mechanochromic, Structurally Colored, and Edible Hydrogels Prepared from Hydroxypropyl Cellulose and Gelatin, *Adv. Mater.*, 2021, **33**, 2102112.

9 W. Liu, X. Wang, R. Li, S. Sun, Z. Li, J. Hao, B. Lin, H. Jiang and L. Xie, A Precise Molecular Design to Achieve ACQ-to-AIE Transformation for Developing New Mechanochromic Material by Regio-Isomerization Strategy, *ChemistrySelect*, 2022, **7**, e202104111.

10 Y. Fang, L. Zhang, Y. Yu, X. Yang, K. Wang and B. Zou, Manipulating Emission Enhancement and Piezochromism in Two-Dimensional Organic-Inorganic Halide Perovskite $[(HO)(CH_2)2NH_3]2PbI_4$ by High Pressure, *CCS Chem.*, 2020, **3**, 2203–2210.

11 Z. Ma, F. Li, D. Zhao, G. Xiao and B. Zou, Whether or Not Emission of Cs4PbBr6 Nanocrystals: High-Pressure Experimental Evidence, *CCS Chem.*, 2020, **2**, 71–80.

12 X. Wang, Q. Liu, H. Yan, Z. Liu, M. Yao, Q. Zhang, S. Gong and W. He, Piezochromic luminescence behaviors of two new benzothiazole–enamido boron difluoride complexes: intra- and inter-molecular effects induced by hydrostatic compression, *Chem. Commun.*, 2015, **51**, 7497–7500.

13 X. Wang, C. Qi, Z. Fu, H. Zhang, J. Wang, H. T. Feng, K. Wang, B. Zou, J. W. Y. Lam and B. Z. Tang, A synergy between the push–pull electronic effect and twisted conformation for high-contrast mechanochromic AIEgens, *Mater. Horiz.*, 2021, **8**, 630–638.

14 Y. Xiong, J. Huang, Y. Liu, B. Xiao, B. Xu, Z. Zhao and B. Z. Tang, High-contrast luminescence dependent on polymorphism and mechanochromism of AIE-active (4-(phenothiazin-10-yl)phenyl)(pyren-1-yl)methanone, *J. Mater. Chem. C*, 2020, **8**, 2460–2466.

15 L. Wang, K. Wang, B. Zou, K. Ye, H. Zhang and Y. Wang, Luminescent Chromism of Boron Diketonate Crystals: Distinct Responses to Different Stresses, *Adv. Mater.*, 2015, **27**, 2918–2922.

16 Y. Dong, B. Xu, J. Zhang, X. Tan, L. Wang, J. Chen, H. Lv, S. Wen, B. Li, L. Ye, B. Zou and W. Tian, Piezochromic Luminescence Based on the Molecular Aggregation of 9,10-Bis((E)-2-(pyrid-2-yl)vinyl)anthracene, *Angew. Chem., Int. Ed.*, 2012, **51**, 10782–10785.

17 K. Nagura, S. Saito, H. Yusa, H. Yamawaki, H. Fujihisa, H. Sato, Y. Shimoikeda and S. Yamaguchi, Distinct Responses to Mechanical Grinding and Hydrostatic Pressure in Luminescent Chromism of Tetrathiazolylthiophene, *J. Am. Chem. Soc.*, 2013, **135**, 10322–10325.

18 Y. Liu, Q. Zeng, B. Zou, Y. Liu, B. Xu and W. Tian, Piezochromic Luminescence of Donor–Acceptor Cocrystals: Distinct Responses to Anisotropic Grinding and Isotropic Compression, *Angew. Chem., Int. Ed.*, 2018, **57**, 15670–15674.

19 H. Yuan, K. Wang, K. Yang, B. Liu and B. Zou, Luminescence Properties of Compressed Tetraphenylethene: The Role of Intermolecular Interactions, *J. Phys. Chem. Lett.*, 2014, **5**, 2968–2973.

20 Y. Gu, H. Liu, R. Qiu, Z. Liu, C. Wang, T. Katsura, H. Zhang, M. Wu, M. Yao, H. Zheng, K. Li, Y. Wang, K. Wang, B. Yang, Y. Ma and B. Zou, Pressure-Induced Emission Enhancement and Multicolor Emission for 1,2,3,4-Tetraphenyl-1,3-

cyclopentadiene: Controlled Structure Evolution, *J. Phys. Chem. Lett.*, 2019, **10**, 5557–5562.

21 J. Wu, H. Wang, S. Xu and W. Xu, Comparison of Shearing Force and Hydrostatic Pressure on Molecular Structures of Triphenylamine by Fluorescence and Raman Spectroscopies, *J. Phys. Chem. A*, 2015, **119**, 1303–1308.

22 Y. Gu, K. Wang, Y. Dai, G. Xiao, Y. Ma, Y. Qiao and B. Zou, Pressure-Induced Emission Enhancement of Carbazole: The Restriction of Intramolecular Vibration, *J. Phys. Chem. Lett.*, 2017, **8**, 4191–4196.

23 S. Zhang, Y. Dai, S. Luo, Y. Gao, N. Gao, K. Wang, B. Zou, B. Yang and Y. Ma, Rehybridization of Nitrogen Atom Induced Photoluminescence Enhancement under Pressure Stimulation, *Adv. Funct. Mater.*, 2017, **27**, 1602276.

24 Q. Qi, J. Qian, X. Tan, J. Zhang, L. Wang, B. Xu, B. Zou and W. Tian, Remarkable Turn-On and Color-Tuned Piezochromic Luminescence: Mechanically Switching Intramolecular Charge Transfer in Molecular Crystals, *Adv. Funct. Mater.*, 2015, **25**, 4005–4010.

25 A. B. Cairns and A. L. Goodwin, Negative linear compressibility, *Phys. Chem. Chem. Phys.*, 2015, **17**, 20449–20465.

26 W. Li, M. R. Probert, M. Kosa, T. D. Bennett, A. Thirumurugan, R. P. Burwood, M. Parinello, J. A. K. Howard and A. K. Cheetham, Negative Linear Compressibility of a Metal–Organic Framework, *J. Am. Chem. Soc.*, 2012, **134**, 11940–11943.

27 A. B. Cairns, J. Catafesta, C. Levelut, J. Rouquette, A. van der Lee, L. Peters, A. L. Thompson, V. Dmitriev, J. Haines and A. L. Goodwin, Giant negative linear compressibility in zinc dicyanoaurate, *Nat. Mater.*, 2013, **12**, 212–216.

28 L. Goodwin Andrew, A. Keen David and G. Tucker Matthew, Large negative linear compressibility of $Ag_3[Co(CN)_6]$, *Proc. Natl. Acad. Sci.*, 2008, **105**, 18708–18713.

29 Y. Qiao, K. Wang, H. Yuan, K. Yang and B. Zou, Negative Linear Compressibility in Organic Mineral Ammonium Oxalate Monohydrate with Hydrogen Bonding Wine-Rack Motifs, *J. Phys. Chem. Lett.*, 2015, **6**, 2755–2760.

30 Q. Zeng, K. Wang and B. Zou, Large Negative Linear Compressibility in InH(BDC)2 from Framework Hinging, *J. Am. Chem. Soc.*, 2017, **139**, 15648–15651.

31 Y. Zhao, C. Fan, C. Pei, X. Geng, G. Xing, T. Ben and S. Qiu, Colossal Negative Linear Compressibility in Porous Organic Salts, *J. Am. Chem. Soc.*, 2020, **142**, 3593–3599.

32 P. S. Ghosh and I. Ponomareva, Negative Linear Compressibility in $[NH_3NH_2]Co(HCOO)_3$ and Its Structural Origin Revealed from First Principles, *J. Phys. Chem. Lett.*, 2021, **12**, 7560–7565.

33 O. Laporte and W. F. Meggers, Some Rules of Spectral Structure, *J. Opt. Soc. Am.*, 1925, **11**, 459–463.

34 Z. Szakács and E. Vauthey, Excited-State Symmetry Breaking and the Laporte Rule, *J. Phys. Chem. Lett.*, 2021, **12**, 4067–4071.

35 S. K. Behera, S. Y. Park and J. Gierschner, Dual Emission: Classes, Mechanisms, and Conditions, *Angew. Chem., Int. Ed.*, 2021, **60**, 22624–22638.

36 I. O. Osorio-Roman, V. Vargas C and R. F. Aroca, Vibrational and Surface-Enhanced Raman Spectra of 1,6-Diphenyl-1,3,5-hexatriene, *Appl. Spectrosc.*, 2007, **61**, 1001–1006.

37 S. Choi and T. G. Spiro, Out-of-plane deformation modes in the resonance Raman spectra of metalloporphyrins and heme proteins, *J. Am. Chem. Soc.*, 1983, **105**, 3683–3692.

38 C. A. Cooper, R. J. Young and M. Halsall, Investigation into the deformation of carbon nanotubes and their composites through the use of Raman spectroscopy, *Composites, Part A*, 2001, **32**, 401–411.

39 P. Atkins, P. W. Atkins and J. de Paula, *Atkins' physical chemistry*, Oxford university press, 2014.

40 C. Feng, K. Wang, Y. Xu, L. Liu, B. Zou and P. Lu, Unique piezochromic fluorescence behavior of organic crystal of carbazole-substituted CNDSB, *Chem. Commun.*, 2016, **52**, 3836–3839.

41 J. Guan, X. Tang, C. Zhang, K. Li, X. Lin, L. Wang, H. H. Lee, J. Xu, H. Zheng and H. K. Mao, Consecutive and Extensive Transition of Luminescent Color of an Organic Solid Material by Applying High Pressure, *J. Phys. Chem. C*, 2020, **124**, 14911–14917.

42 H. Yang, Z. Sun, C. Lv, M. Qile, K. Wang, H. Gao, B. Zou, Q. Song and Y. Zhang, Ratiometric Piezochromism of Electrospun Polymer Films: Intermolecular Interactions for Enhanced Sensitivity and Color Difference, *ChemPlusChem*, 2018, **83**, 132–139.

43 Z. Fu, H. Liu, J. Zhao, X. Zhang, X. Zheng, B. Yang, X. Yang, K. Wang and B. Zou, Pressure-induced emission enhancement by restricting chemical bond vibration, *J. Mater. Chem. C*, 2021, **9**, 14578–14582.

44 M. A. Spackman and D. Jayatilaka, Hirshfeld surface analysis, *CrystEngComm*, 2009, **11**, 19–32.

45 M. J. Cliffe and A. L. Goodwin, PASCal: a principal axis strain calculator for thermal expansion and compressibility determination, *J. Appl. Crystallogr.*, 2012, **45**, 1321–1329.

46 A. D. Fortes, E. Suard and K. S. Knight, Negative Linear Compressibility and Massive Anisotropic Thermal Expansion in Methanol Monohydrate, *Science*, 2011, **331**, 742–746.